Ultramicroscopy 159 (2015) 95–100

Contents lists available at ScienceDirect

Ultramicroscopy

journal homepage: www.elsevier.com/locate/ultramic

Short communication

Vibrational-loss EELS and the avoidance of radiation damage

R.F. Egerton

Physics Department, University of Alberta, Edmonton, Canada T6G 2E1

ARTICLE INFO

Article history:
Received 13 May 2015
Received in revised form
14 August 2015
Accepted 23 August 2015
Available online 28 August 2015

Keywords:
Electron energy-loss spectroscopy
Radiation damage
Phonons
STEM
Monochromator
Vibrational energy loss

ABSTRACT

We discuss vibrational-mode energy-loss spectroscopy using an aloof beam of electrons positioned a small distance b from the edge of a specimen in a probe-forming TEM or STEM equipped with a high-resolution monochromator. Due to the delocalization of inelastic scattering, a strong vibrational-loss signal can be recorded without causing significant damage to a beam-sensitive specimen. Calculations for $b=20$ nm suggest that damage is reduced by typically a factor of 1000 (relative to electrons of the same energy transmitted through the specimen) for the same signal strength and spatial resolution. About 50% of the vibrational-loss signal comes from material lying within a distance b of the edge of the specimen and extending over a length $2.5b$ parallel to the edge. Although energy-filtered imaging appears impossible in aloof mode, an undersampling STEM technique is proposed, taking advantage of scattering delocalization to obtain a vibrational-loss image that leaves most of the imaged area undamaged.

1. Introduction

Improved monochromator designs have made possible electron energy-loss spectroscopy in a transmission electron microscope (TEM-EELS) with an energy resolution down to about 10 meV [1]. This capability allows local measurement of defect states within the band gap of semiconductors and insulators [2] together with more accurate measurement of energy gaps [3]. It also permits vibrational-mode energy-loss spectroscopy (vibEELS), with the prospect of obtaining atomic-bonding information similar to that provided by infrared spectroscopy or reflection-mode high-resolution energy-loss spectroscopy (HREELS) but at higher spatial resolution. Related tip-based spectroscopies also provide high resolution [4] but they typically sample only a thin surface layer, whereas transmission techniques extract information from within the interior of a specimen. In addition, TEM-EELS covers a wide range of energy loss (equivalent to infra-red up to x-ray photon energies) and allows diffraction and other techniques to be used in the same instrument.

Transmission-mode vibEELS data was obtained many years ago by Boersch, Geiger and colleagues, initially from gases [5–7] and then from various types of solid specimen [8–11], using an apparatus that generated a 30-keV beam of electrons with a diameter of the order of 10 μm. Use of a conventional or scanning TEM allows similar data to be obtained from much smaller regions of specimen, within the limitations imposed by radiation damage and by delocalization of inelastic scattering [12]. Although delocalization is often a disadvantage, we discuss in this paper how it can be beneficial in reducing the radiation damage that would otherwise occur in beam-sensitive specimens, consistent with recent experimental findings [1,31,34].

2. Delocalization of inelastic scattering

Using 33-keV electrons and gaseous samples of CO_2, N_2O and C_2H_4, Geiger and Wittmaack [7] measured scattering cross sections for several vibrational peaks, using a very small collection aperture (semiangle $\beta=0.11$ mrad). These cross sections were within a factor of two of those calculated using dipole theory, which predicts a Lorentzian angular distribution of intensity: $dI/d\Omega \propto 1/(\theta^2+\theta_E^2)$, whose halfwidth is the characteristic angle $\theta_E \approx E/(2E_0)$. For $E < 0.5$ eV and an incident-electron energy $E_0 = 60$ keV, θ_E is less than 5 μrad and as a result of this very narrow angular width, the scattering is expected to be relatively delocalized.

To understand why, suppose θ_{50} is the median angle of inelastic scattering, such that half of the scattered electrons acquire a transverse momentum within the range $\Delta p_x = \pm(h/\lambda)\theta_{50}$, where λ is the de Broglie wavelength of the incident electrons and h is the Planck constant. The Heisenberg uncertainty relation ($\Delta p_x\, \Delta x \approx h$) then suggests that the region scattering 50% of the electrons cannot be defined to better than about $L_{50} \approx \Delta x \approx (0.5)\lambda/\theta_{50}$. Alternatively, the Rayleigh criterion can be used to predict a delocalization distance of $L_{50} \approx (0.6)\lambda/\theta_{50}$. For an angular distribution that is Lorentzian up to θ_c and then falls off much more rapidly, the median scattering angle is $\theta_{50} \approx (\theta_E\theta_c)^{1/2}$. The *observed* value of L_{50} is of the order of 100 nm for $E_0=60$ keV and $E \approx 0.15$ eV (a

E-mail address: regerton@ualberta.ca

http://dx.doi.org/10.1016/j.ultramic.2015.08.003
0304-3991/

typical vibrational-peak energy), implying an effective cutoff angle $\theta_c \approx 0.65$ mrad $\approx 500\ \theta_E$. For comparison, θ_c/θ_E is of the order of 100 for plasmon losses and in the range 10–50 for most inner-shell losses.

Scattering delocalization is characterized more completely in terms of a point-spread function (PSF). For a Lorentzian angular distribution with a cutoff at a high scattering angle, Fourier analysis suggests [13] that this PSF is also approximately Lorentzian, with a sharp central maximum and a long tail whose intensity is proportional to $1/r^2$, where r represents radial distance from the primary-electron path. This tail extends up to the Bohr adiabatic limit $b_{max}=\gamma hv/(2\pi E)$, beyond which the intensity falls exponentially [40]. For small E, the tail contains much of the intensity, leading to a large value of L_{50}, whereas the sharp central peak offers the possibility of high image resolution [14], analogous to the atomic resolution seen in secondary-electron images recorded using a thin specimen and an aberration-corrected STEM [15–17].

There is also a possibility that non-dipole scattering (known as impact scattering in the HREELS community), whose angular distribution is broad, may provide high spatial resolution [18–22]. Indeed, recent calculations [23–26] have predicted atomic resolution from vibrational losses, subject to adequate signal/noise ratio and the absence of radiation damage. However, making use of this signal requires energy-loss spectroscopy at high scattering angles, which is technically difficult (especially at 20 meV resolution) because of spectrometer and lens aberrations. So far, vibrational spectroscopy in the STEM has used collection angles up to 15 mrad and under such conditions dipole scattering appears to predominate.

3. Aloof-beam spectroscopy

If a finely focused STEM probe is positioned at a small distance b (known as the impact parameter) just beyond the edge of the specimen, an energy-loss spectrum can be recorded in the so-called aloof mode [1,27,35,36]. This spectrum is heavily weighted towards energy-loss processes whose delocalization distance is comparable to or larger than the impact parameter. Surface losses tend to predominate over bulk losses and vibrational peaks are particularly favored, due to their large delocalization distance. Elastic scattering should have negligible effect on the aloof spectrum because its angular distribution is broad and the delocalization distance correspondingly small.

One perceived advantage of aloof mode is that radiation damage (radiolysis) to beam-sensitive materials may be reduced [32–35]. This idea was originally based on the possibility that damage to aromatic organic compounds might require K-shell excitation, implying $E > 280$ eV (corresponding to $L_{50} < 0.3$ nm). However vibEELS spectroscopy presents a more compelling case for aloof spectroscopy, since the energy losses involved correspond to $L_{50} \approx 100$ nm, compared to $L_{50} < 5$ nm for the valence-shell excitation ($E > 5$ eV) that causes radiolysis in most beam-sensitive materials. For this reason, energy-loss spectra of hydrides and nucleic acids have been recorded in aloof-beam mode [1,31,34]. However, no quantitative measurements of the benefit of aloof mode are available, so this paper aims to evaluate the situation by means of simple calculations.

Knock-on displacement damage (which predominates in electrically conducting specimens) arises from large-angle elastic collisions and the corresponding delocalization distance has subatomic dimensions. As a result, knock-on damage should be completely absent in aloof mode.

4. Dielectric formulation of energy loss

Yet another description of delocalization is provided by dielectric theory, in which energy-loss intensity is related to the photon-energy dependence of the complex relative permittivity $\varepsilon(E)$. For aloof-beam spectroscopy, the inelastic-scattering probability (per unit energy loss E) is [27]

$$\mathrm{dP/\ dE} = (t/a_0)(\pi T)^{-1} Im\{-2/[\varepsilon(E)+1]\} K_0(4\pi bE/[\gamma vh]) \quad (1)$$

where t is the specimen thickness, $a_0=0.0259$ nm is the Bohr radius, m_0 is the electron rest mass, v is the incident-electron speed, $\gamma = 1/(1-v^2/c^2)^{1/2}$ and $T=m_0v^2/2=(E_0/\gamma^2)(1+\gamma)/2$, equal to 50.9 keV for an incident energy $E_0=60$ keV. The function K_0 (a zero-order Bessel function of second kind) represents the dependence of the inelastic signal on the distance b between the electron probe and the edge of the specimen. In the case of vibrational losses, this K_0-dependence has been found to be consistent with measurements [1].

In Fig. 1, the b-dependence of Eq. (1) is shown on a logarithmic scale, for $E = 0.1$ eV and 0.4 eV (defining the region containing most vibEELS peaks) and for a typical valence-electron loss ($E = 20$ eV). Comparison of these curves illustrates how the vibEELS signal persists at much larger impact parameters than the valence-loss signal, as seen experimentally [1].

Although the K_0 function has an exponential tail, the straight-line behavior in Fig. 1 reveals that dP/dE approximates to a logarithmic function over most of its useful range, and we can argue that this behavior is consistent with the r^{-2} dependence of the inelastic-scattering PSF. Considering a small range 2ϕ of azimuthal angles about an x-axis drawn through the probe and perpendicular to the edge of the specimen (Fig. 2), the energy-loss probability is approximately $dP/dE \propto \int r^{-2}(2\phi\, r)\, dr \propto \log(r_{max}) - \log(b)$.

As seen in Fig. 1, a nearly logarithmic b-dependence is also expected for valence-electron (plasmon) scattering and experimental evidence for this behavior is given in Fig. 3. In this case, the data were acquired with an aloof STEM probe by Zhou et al. [28] and are here replotted with a logarithmic distance scale. This experimental verification supports the assumptions we will use to calculate damage rates and the spatial resolution of aloof-mode spectroscopy.

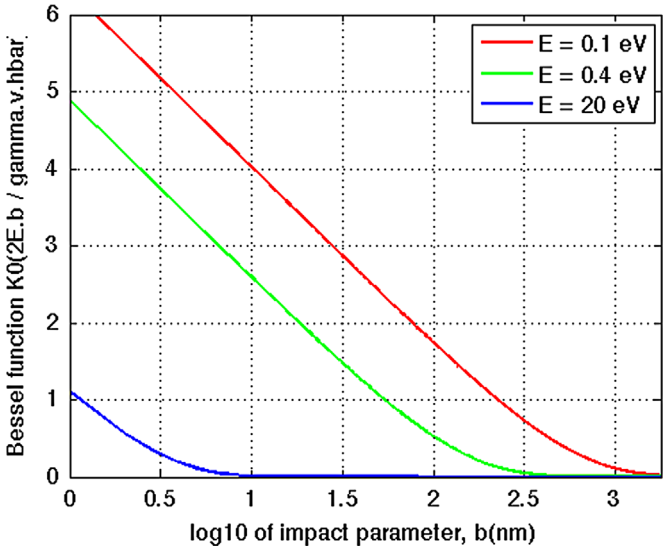

Fig. 1. Bessel function $K_0(4\pi bE/[\gamma vh])$ plotted as a function of $\log_{10}(b)$, showing how the intensity of inelastic scattering at three energy losses (0.1 eV, 0.4 eV and 20 eV) varies with the impact parameter b of an aloof probe of 60 keV electrons. (For interpretation of the references to color in this figure, the reader is referred to the web version of this article.)

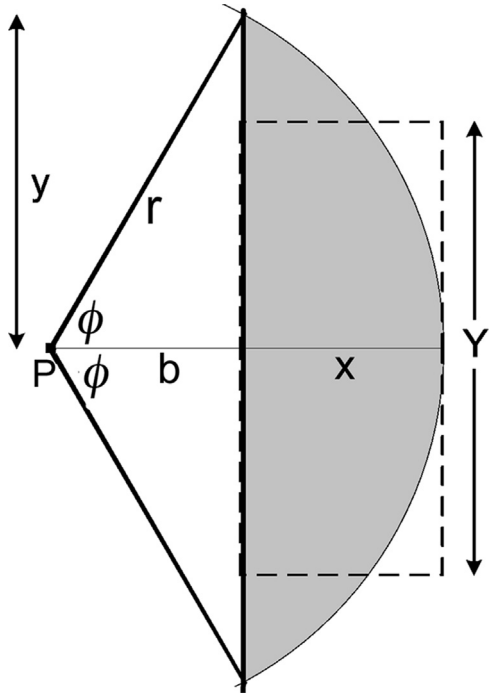

Fig. 2. Geometry for an aloof probe of electrons P, relative to the edge of the specimen (vertical *y*-axis). Dashed lines outline an area equal to the shaded area that represents regions of specimen that lie within a distance r $(=b+x)$ of the probe.

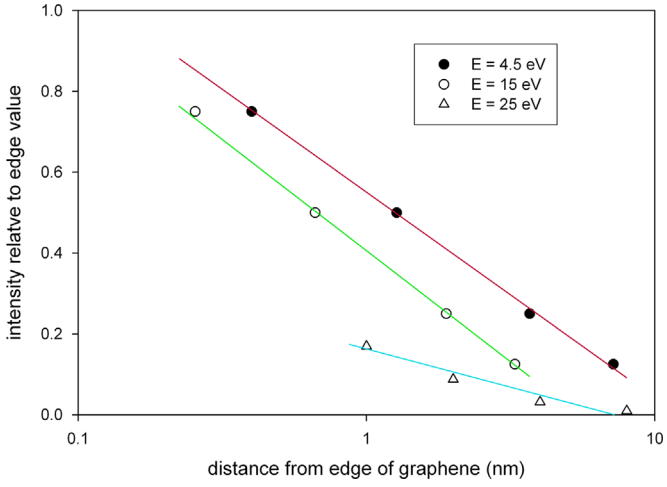

Fig. 3. Energy-loss intensity at three values of energy loss E, measured by Zhou et al. [28] with an aloof probe of 60 keV electrons (diameter about 0.1 nm) held at various distances from the edge of a monolayer graphene sheet. The horizontal impact-parameter scale is logarithmic.

Fig. 4 shows the integrated intensity P_a of an aloof vibrational-loss peak (E = 0.15 eV) divided by the corresponding probability P_t for the same electrons transmitted *through* the specimen. For 60 keV electrons and an impact parameter of 20 nm, the aloof signal is about 25% of the transmitted value. Increasing the incident energy to 200 keV decreases both P_a and P_t but slightly increases the ratio P_a/P_t (red curve in Fig. 1b) for impact parameters above 3 nm. This behavior is consistent with a delocalization length L_{50} that increases weakly with increasing incident energy [13].

5. Radiation damage

Unfortunately, many specimens of interest for vibrational-mode EELS are radiation-sensitive. For example, organic materials degrade rapidly as a result of ionization damage (radiolysis), which arises from the energy transferred to the specimen as a result of inelastic scattering. Unlike the case of knock-on displacement damage, which predominates in an electrically conducting specimen, there is no incident-energy threshold (above 1 keV, as required for transmission measurements) below which this radiolysis damage disappears. Calculation based on measured vibrational-peak cross sections suggests a dose-limited resolution of about 40 nm, for 60 keV electrons directly incident on a polyethylene specimen [12].

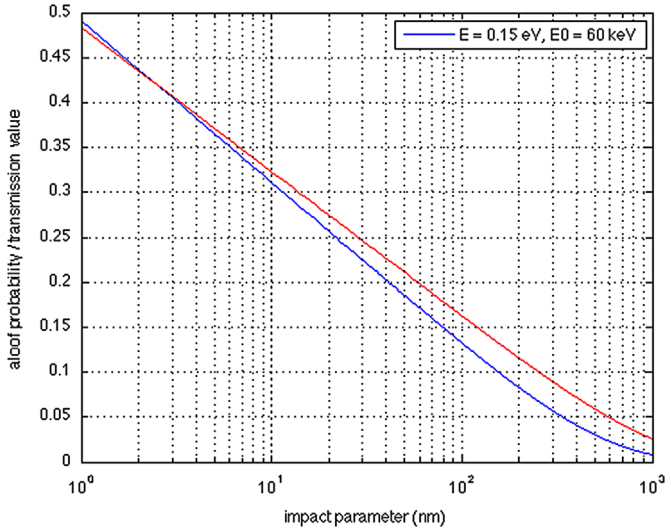

Fig. 4. Relative probability (P_a/P_t) of exciting a vibrational peak (E=0.15 eV) with an aloof probe of impact parameter b, compared to the same probe positioned on the specimen (transmission probability P_t). The lower blue curve is for an incident energy of 60 keV and the upper red curve for an incident energy of 200 keV. (For interpretation of the references to color in this figure legend, the reader is referred to the web version of this article.)

A widely-held belief within the radiation-damage community is that the amount of radiolysis damage (arising from electrons or x-rays) is proportional to the energy deposited in the specimen. In fact, this is the rationale for measuring radiation resistance in terms of Grays (1 Gy=1 J/kg of specimen). However, this rule cannot be exact, since infrared or even visible radiation produces no damage to organic materials unless its intensity is high enough to cause appreciable temperature rise and thermal degradation. So there must be a photon-energy threshold for radiolysis, which has been estimated as 4.8 eV for poly(methyl methacrylate) (PMMA) [29]. The same threshold should apply to radiolysis produced by electrons, since the damage mechanism is similar.

Because vibrational losses have cross sections typically below 1% of valence-loss cross sections and result in an energy exchange that is typically a factor of 100 lower, less than 0.01% of the energy transfer from electrons involves vibrational losses. Moreover, the mean energy loss per inelastic collision exceeds 35 eV for an organic specimen [30], so losses below a 5 eV threshold account for only a small fraction. Consequently, inaccuracy of the deposited-energy rule is likely to be small.

The fact that the energy losses causing damage are typically a factor of 100 larger than vibrational-loss values means that their delocalization distance is at least a factor of 30 smaller (assuming a $L_{50} \propto E^{3/4}$ approximation), as shown also by Fig. 1. This strong E-dependence accounts for the feasibility of aloof-beam spectroscopy with an impact parameter that is small enough to excite an appreciable vibrational-mode signal but large enough to avoid damage.

6. Energy exchange in aloof-beam spectroscopy

To calculate the energy deposited in the specimen by an aloof probe having an impact parameter b, we can use Eq. (1) with the relative permittivity $\varepsilon(E)$ evaluated for energy losses appropriate to valence-electron excitation. For this purpose, we have approximated the dielectric properties of a typical organic material by a Drude expression [13] with a volume energy-loss function centered around E_p=22 eV, the surface energy-loss function $Im\{-2/[\varepsilon(E)+1]\}$ being centered around 16 eV, as shown in Fig. 5.

For energy losses that cause damage to the specimen, the mean energy loss *per aloof primary electron* is

$$E_a = \int (\mathrm{dP/dE})E \, \mathrm{dE} \qquad (2)$$

where dP/dE is given by Eq. (1), the lower limit of integration is the damage-threshold value (taken here as 5 eV) and the upper limit is the primary-beam energy (although a value of 50 eV proved accurate enough for our purposes). Calculations for 60 keV electrons gave E_a = 0.04 eV for b=10 nm, falling to 0.003 eV for b=20 nm; see Fig. 6.

For comparison, the mean energy loss of a 60 keV electron transmitted through a specimen of thickness t is $E_t \approx (t/\lambda_i)E_p$ where $\lambda_i \approx 100$ nm is a mean free path for inelastic scattering and E_p is approximately the plasmon energy, giving E_t = 11 eV for t = 50 nm. So for an aloof probe 20 nm from the specimen edge, the energy deposited is a factor of 3700 smaller than that deposited by the same probe transmitted through the specimen. At this impact parameter, the 0.15 eV vibEELS signal is about 25% of the transmission value (see Fig. 4), so aloof spectroscopy reduces the energy deposition (and damage) by a factor of about 1000 for the same signal. For b = 40 nm, $E_a/E_t \approx 10^{-5}$ and the energy deposition is reduced by a factor of about 20,000 for the same signal. Since E_a and E_t are both proportional to t (in the single-scattering regime), these factors are independent of specimen thickness.

Changing the incident energy from 60 keV to 200 keV decreases E_a at small impact parameter, because of the $1/T$ term in Eq. (1) (equivalent to a reduced inelastic mean free path λ_i). But for $b > 3$ nm, E_a is higher at 200 keV because of the longer delocalization distance and larger value of b_{max}; see Fig. 6. Since 200 keV also gives a smaller vibEELS signal (for $b < 300$ nm) due to the $1/T$ term in Eq. (1), higher incident energy appears disadvantageous for aloof vibrational spectroscopy.

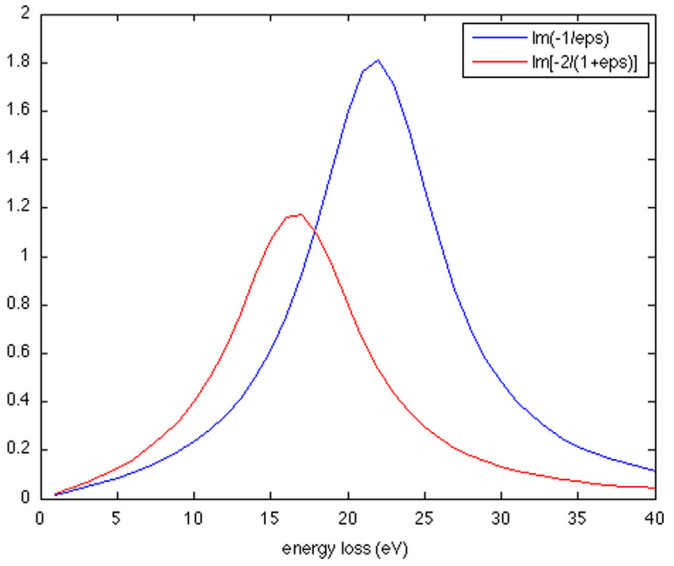

Fig. 5. Bulk (blue) and surface (red) energy-loss functions generated by a Drude formula, appropriate to a typical organic specimen. (For interpretation of the references to color in this figure legend, the reader is referred to the web version of this article.)

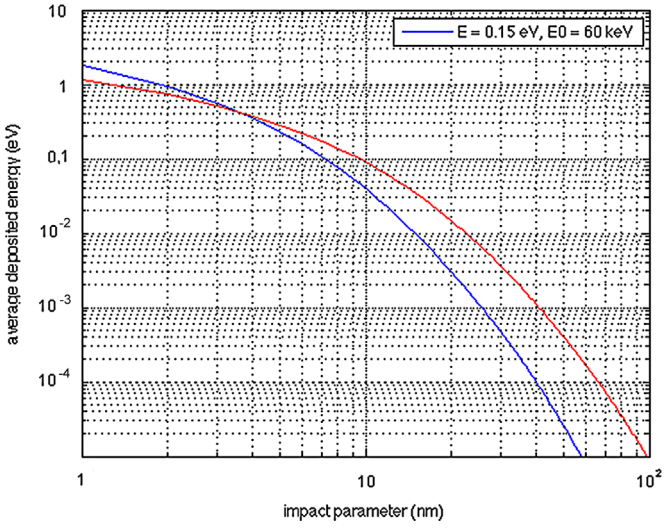

Fig. 6. Mean energy deposited in a 50 nm-thick organic specimen, per 60 keV primary electron (blue curve) or per 200 keV electron (red curve), as a function of the impact parameter of an aloof probe. (For interpretation of the references to color in this figure legend, the reader is referred to the web version of this article.)

7. Spatial distribution of the vibEELS signal and of damage

For a given impact parameter b, we can get an idea of where the vibEELS signal comes from by assuming a $1/r^2$ point-spread function. Considering first the x-dependence, perpendicular to the specimen edge (Fig. 2): the energy-loss intensity is $J(x) \propto C/(x+b)^2$, where C is a constant, giving an integrated intensity $I(x) = \int J(x)\,dx = C(1/b - 1/b_{max}) \approx C/b$, since $b_{max} \approx \gamma hv/(2\pi E)$ is as large as 660 nm for $E \approx 0.15$ eV and $E_0 \approx 60$ keV. The distance x_{50} containing 50% of the signal corresponds to $I(x) = 0.5(C/b)$, resulting in $x_{50} = b$. In other words, the median x-resolution is equal to the impact parameter.

In the direction parallel to the edge of the specimen, a median y-value containing 50% of the signal can be estimated by setting $x = x_{50} = b$, giving $r = 2b$, $\cos(\phi) = b/r = 0.5$, $y = r\sin(\phi) = (3^{1/2})b$; see Fig. 2. Equating the shaded area $A_{50} = \phi r^2 - yb$ to the rectangular area $(Y \cdot x_{50})$ gives Y = 2.46b as the y-range containing half the vibEELS signal.

The spatial resolution of the inelastic signal in aloof mode is therefore dependent on the impact parameter. As the probe is moved away from the edge of the specimen, the area ($\approx 2.5b^2$) contributing half the inelastic signal increases.

Similar arguments should apply to valence-electron losses and the resulting radiolysis damage. As b increases, the deposited energy decreases and this energy is distributed over a larger area adjacent to the edge of the specimen. As a result, the radiation dose decreases dramatically, as shown by the continuous red curve in Fig. 7. Although the vibEELS signal also falls with increasing impact parameter, the signal/dose ratio increases by orders of magnitude (blue dashed curve in Fig. 7).

8. Discussion and conclusions

We have discussed how radiation damage can be largely avoided by performing EELS in aloof-beam mode, with the electron probe at a sufficiently large distance b from the edge of the specimen. In the case of 60 keV electrons and a typical vibrational

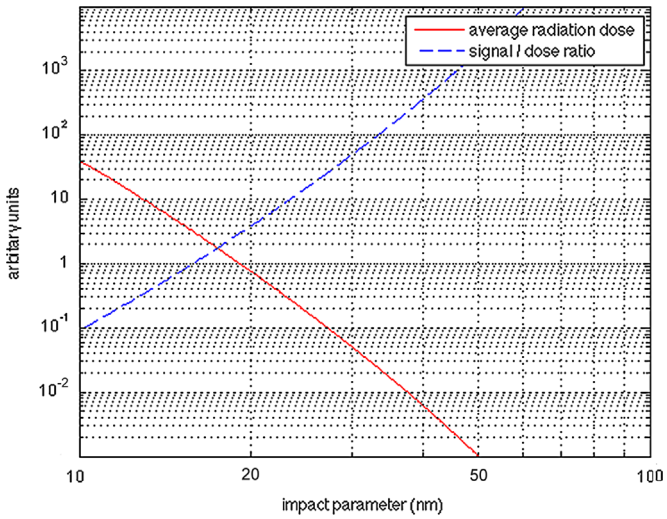

Fig. 7. Median radiation dose (energy per unit area, averaged over an area containing 50% of the signal) and signal/dose ratio for a 0.15 eV energy-loss peak, estimated for an aloof probe of 60 keV electrons. The vertical scale is in arbitary units, so the curves illustrate only the rapid b-dependence of both quantities. (For interpretation of the references to color in this figure, the reader is referred to the web version of this article.)

peak ($E=0.15$ eV), $b \approx 30$ nm may be sufficient to ensure negligible damage. The damage is greater at higher beam energies and the vibEELS signal is lower, for the same impact parameter. Recent measurements do in fact suggest the absence of damage in an organic specimen for an impact parameter of 30 nm and substantial damage when the impact parameter was reduced to 10 nm [31,34,41].

A similar proposal for damage reduction was made in connection with valence-electron spectroscopy, assuming that the radiolysis of some organic specimens might require K-shell excitation, whose broad angular distribution would imply atomic-scale values of the impact parameter [32,33]. Even without this K-shell mechanism, aloof-mode spectroscopy could provide a limited reduction in radiolysis damage when measuring valence-loss peaks with energies substantially lower than the average energy loss, of the order of 40 eV in a thin organic specimen. Such an effect has been reported for the case of the 6 eV π-excitation peak in polystyrene and other polymers, where a small (<100 nm) electron probe produced less damage than expected on the basis of large-probe measurements [37–39].

Practical requirements for aloof spectroscopy include the absence of probe or specimen drift during spectrum acquisition, together with a sufficiently small diameter d and convergence semi-angle α of the probe. Preventing electrons striking the edge of the specimen requires $d < b/2$, $\alpha t/2 < b$ (for a probe focused at the specimen mid-plane) and minimal aberration tails (preferably an aberration-corrected probe).

The requirement $\alpha t/2 < b$ is easy to fulfill: for $\alpha = 30$ mrad and $b = 20$ nm, it implies $t < 1.3$ μm, a condition that is further relaxed in the case of a specimen with a rounded edge. The simulations presented here were based on Eq.(1), which assumes a specimen of uniform thickness t and a sharp (rectangular) edge. Such specimens being rare, the calculated values will only be approximate for real specimens. For the purposes of discussion, we chose a vibEELS peak at 0.15 eV, which is typical of many vibEELS data recorded so far. However, hydrogen can give a vibrational peak at 0.45 eV (O–H stretch mode) [34], implying a rather more rapid falloff of signal away from the edge of the specimen (see Fig. 1). Even so, an impact parameter in the range 20–30 nm should give an adequate signal and considerably less damage than a transmission measurement.

One disadvantage of aloof-beam spectroscopy is that the spatial resolution is limited to a value of the order of the impact parameter of the probe. However, a similar limit (a few tens of nanometer for vibEELS data, determined by delocalization and radiation damage) applies in the case where electrons are transmitted through the specimen.

Another disadvantage is the inability of an aloof beam to form energy-filtered images of the specimen. However, it should be possible to take advantage of the delocalization of inelastic scattering in *transmission mode*, by forming an energy-selected STEM image with a digital raster having an interpixel spacing (maybe100 nm) much larger than the probe diameter. In this undersampling condition, radiolysis damage should be produced only within a few nanometers of each probe position. The vibEELS signal would arise mainly from the intervening undamaged material, a large fraction of the scanned area remaining undamaged.

Concerning the nature of vibrational energy losses in an amorphous or molecular solid, these features may be thought of as involving the stretching or bending of individual chemical bonds. In the case of a crystal, it is more usual to think in terms of acoustic and optical phonons, but these are likely to be surface phonons in a TEM specimen of typical thickness [21]. If so, the transmission-mode vibEELS losses will be excited mainly while the beam electrons are traveling in vacuum (approaching and leaving the specimen), just as in the case of aloof-probe spectroscopy.

Because of the low energies and long wavelengths of phonons compared to plasmons, surface phonons on the two surfaces of a specimen will be closely coupled. In the plasmon case, surface-excitation peaks occur at energies substantially below the bulk-resonance energy, whereas the observed vibEELS peaks have energies quite close to the bulk values given by infrared spectroscopy [1,5–11]. An explanation may lie in the fact that vibrational excitations are more akin to single-electron losses than to plasmons, their peak energies being defined by the imaginary part ε_2 of the permittivity, rather than by a free-electron resonance.

Acknowledgments

The author thanks Archie Howie, Matt Libera, Peter Rez, Ondrej Krivanek and Peter Crozier for helpful discussions, and the Natural Sciences and Engineering Research Council of Canada (RGPIN-348) for financial support.

References

[1] O.L. Krivanek, T.C. Lovejoy, N. Dellby, T. Aoki, R.W. Carpenter, P. Rez, E. Soignard, J. Zhu, P.E. Batson, M.J. Lagos, R.F. Egerton, P.A. Crozier, Nature 514 (2014) 209.
[2] T. Aoki, L.A.J. Garvie, P. Rez, Ultramicroscopy 153 (2015) 40.
[3] R.W. Carpenter, H. Xie, T. Aoki, F.A. Ponce, Microsc. Microanal. 21 (Suppl. 3) (2015) S657.
[4] (a) P. Dorozhkin, E. Kuznetsov, A. Schokin, S. Timofeev, V. Bykov, Microsc. Today 18 (2010) 28;
(b) E.C. Le Ru, P.G. Etchegoin, MRS Bull. 38 (2013) 631.
[5] H. Boersch, J. Geiger, H. Hellwig, Phys. Lett. 3 (1962) 64.
[6] H. Boersch, J. Geiger, W. Stickel, Phys. Lett. 3 (1964) 285.
[7] J. Geiger, K. Wittmaack, Z. Phys. 187 (1965) 433.
[8] H. Boersch, J. Geiger, W. Stickel, Phys. Rev. Lett. 17 (1966) 379.
[9] B. Schröder, J. Geiger, Phys. Rev. Lett. 28 (1972) 301.
[10] J. Geiger, H. Katterwe, Thin Solid Films 32 (1976) 359.
[11] J. Geiger, H. Katterwe, Z. Phys. 29 (1978) 113.
[12] R.F. Egerton, Microsc. Microanal. 20 (2014) 658.
[13] R.F. Egerton, Electron Energy-Loss Spectroscopy in the Electron Microscope, 3rd edition, Springer, New York (2011), p. 226.
[14] W. Zhou, J. Lee, J. Nanda, S.T. Pantelides, S.J. Pennycook, J.-C. Idrobo, Nature Nanotechnol. 7 (2012) 161.
[15] H. Inada, D. Su, R.F. Egerton, M. Konno, L. Wu, J. Ciston, J. Wall, Y. Zhu, Ultramicroscopy 111 (2011) 865.
[16] A. Howie, R.H. Milne, Ultramicroscopy 18 (1985) 427.

[17] J. Drucker, M.R. Scheinfein, J. Liu, J.K. Weiss, J. Appl. Phys. 74 (1993) 7329.
[18] H. Ibach, D.L. Mills, Electron Energy Loss Spectroscopy and Surface Vibrations, Academic Press, London (1982), p. 1473.
[19] H. Ibach, Physics of Surfaces and Interfaces, Springer-Verlag, Berlin, 2006, ISBN-13 978-3-540- 34709-5.
[20] P.A. Thiry, M. Liehr, J.J. Pireaux, R. Caudano, Phys. Scr. 35 (1987) 368.
[21] A.A. Lucas, M. Sunjic, Prog. Surf. Sci. 2 (1972) 75.
[22] A. Howie, Ultramicroscopy 151 (2015) 116.
[23] P. Rez, Microsc. Microanal. 20 (2014) 671.
[24] C. Dwyer, Phys. Rev. B 89 (2014) 054103.
[25] P. Cueva, D.A. Muller, Microsc. Microanal. 20 (Suppl. 3) (2014) S590.
[26] N.R. Lugg, B.D. Forbes, S.D. Findlay, L.J. Allen, Phys. Rev. B 91 (2015) 144108.
[27] A. Howie, Ultramicroscopy 11 (1983) 141.
[28] W. Zhou, S.J. Pennycook, J.-C. Idrobo, Ultramicroscopy 12 (2012) 51.
[29] B.J. Lin, J. Vac. Sci. Technol. 12 (1975) 1317.
[30] Z. Tan, Y. Xia, M. Zhao, X. Liu, F. Li, B. Huang, Y. Ji, Nucl. Instrum. Methods B 222 (2004) 27.
[31] H. Cohen, P. Rez, T. Aoki, P.A. Crozier, N. Dellby, Z. Dellby, D. Gur, T.C. Lovejoy, K. March, M.C. Sarahan, S.G. Wolf, O.L. Krivanek., Microsc. Microanal. 21 (Suppl. 3) (2015) S661.
[32] A. Howie Echenique, R.H. Ritchie, Phys. Rev. Lett. 83 (1999) 658.
[33] M.G. Walls, A. Howie, Ultramicroscopy 28 (1989) 40.
[34] P.A. Crozier, T. Aoki, Q. Liu, L. Zhang, Microsc. Microanal 21 (Suppl. 3) (2015) S1473.
[35] H. Cohen, T. Maniv, R. Tenne, Y. Rosenfeld Hakohen, O. Stephan, C. Colliex, Phys. Rev. Lett. 80 (1998) 782 83 (1999) 659.
[36] B.W. Reed, M. Sarikaya, Phys. Rev. B 64 (2001) 195404.
[37] R.F. Egerton, S. Lazar, M. Libera, Micron 43 (2012) 2.
[38] K. Siangchaew, M. Libera, Philos. Mag. A 80 (2000) 1001.
[39] K. Varlot, J.M. Martin, C. Quet, Y. Kihn, Ultramicroscopy 68 (1997) 123.
[40] D.A. Muller, J. Silcox, Ultramicroscopy 59 (1995) 195.
[41] Peter Rez, Toshi Aoki, Katia March, Dvir Gur, Ondrej Krivanek, Niklas Dellby, Tracy C. Lovejoy, Sharon G. Wolf and Hagai Cohen, submitted for publication.